Electro-catalytic performance of nickel hydroxide decorated microporous nanozeolite Beta modified carbon paste electrode for formaldehyde oxidation

Samira Eshagh-Nimvari
Seyed Karim Hassaninejad-Darzi (hassaninejad@nit.ac.ir)
Babol Noshirvani University of Technology https://orcid.org/0000-0002-9697-0874

Research Article

Keywords: Nanozeolite Beta, Ni¬¬(OH)2-Beta/CPE, Electro-catalytic oxidation, Formaldehyde

Posted Date: April 18th, 2022

DOI: https://doi.org/10.21203/rs.3.rs-1537328/v1

Abstract

In this paper, aluminosilicate nanozeolite beta has been prepared and completely described using X-ray diffraction (XRD), nitrogen sorption isotherm, Fourier transform infrared (FT-IR), transmission electron micrograph (TEM) and field emission scanning electronic microscopy (FESEM) techniques. TEM image of synthesized nanozeolite demonstrates semispherical particles with a uniform morphology and dimensions under 50 nm. The BET surface area, total pore volume and pore diameter of it were attained to be 321 $m^2\ g^{-1}$, 0.053 $cm^3\ g^{-1}$ and 1.22 nm, respectively. The modified carbon paste electrode by aluminosilicate nanozeolite beta and nickel hydroxide ($Ni(OH)_2$-Beta/CPE) was applied for formaldehyde (HCHO) electro-catalytic oxidation in the alkaline media. The obtained results specify that $Ni(OH)_2$-Beta/CPE demonstrates worthy electro-catalytic activity for oxidation of HCHO due to mesoporous construction and the great surface area of nanozeolite beta. The electron-transfer coefficient, catalytic rate constant and diffusion coefficient are found to be 0.69, $2.08\times10^6\ cm^3\ mol^{-1}\ s^{-1}$ and $4.4\times10^{-7}\ cm^2\ s^{-1}$, respectively. The $Ni(OH)_2$-Beta/CPE exhibited good reproducibility and stability and it has low price, low background current, simplicity of surface renewal. This modified electrode has better poisoning tolerance capability than bare CPE for HCHO electro-catalytic oxidation and is a higher device for the long term accomplishment.

1 Introduction

With the rapid progress of the economy and society, the energy crisis of old sources which produced environmental contamination has converted progressively serious. In this progressively environmentally sensible time, we have revolved our responsiveness to green renewable energy. However, effective adaptation and storage of chemical energy have developed one of the major challenges [1, 2]. The electro-catalytic oxidation of methanol (CH_3OH) and formaldehyde (HCHO) is a reaction topic to intense exploration because of its potential presentation in fuel cell technology [3]. Although, HCHO is a damaging material and not exact appropriate for the fuel cells, but the knowledge of its electro-oxidation is significant for the full considerate of CH_3OH electro-oxidation in direct methanol fuel cells (DMFCs), because it is formed by fractional oxidation of CH_3OH [4]. The HCHO be able to apply as a process for eliminating and alteration of it to fewer poisonous materials from dilute waste streams [5, 6].

Literature review exhibits that important attention has been engrossed in the electro-oxidation of HCHO for many years [4, 7–11]. Various components have been used for the HCHO electro-oxidation containing Pd electrode [12], Pt nanoparticles/GCE [13], Pt electrode [14], Pt-MnO_2 [15], Cu electrode [6], Cu-Pd [3], Cu/Pd/MWCNTs/CPE [16], Pt–Pd/CNT [17], Au nanoparticles [18], rGO/ZnO composite [19], nickel phosphate/GCE [5], Ni-Pd/GCE [20], nickel phosphate/carbon composite [21], Ni thin film on SiO_2/Au [22], $Ni(OH)_2$-Pt/Al_2O_3 [23], $Ni(OH)_2$-MIL/CPE [24] and zeolite-modified electrodes containing $Ni(OH)_2$ [25–30]. However, several of above devices were established to undergo the difficulties of little sensitivity and poor selectivity shaped by surface damaging from the adsorbed intermediate. It is significant to progress a new electrode which has great sensitivity and stability for the HCHO electro-oxidation.

Zeolites have identical network size and exceptional molecular form selectivity, and robust acidity and worthy hydrothermal and thermal stability. The BEA class of zeolite include of an intergrowth of 2 or additional

polymorphs involved of a 3-dimensional system of 12 membered ring networks [31]. Zeolite beta framework topology has benefit for example great accessible micropore volume, large pore channel and the existence of energetic locations that progress metal zeolite interaction by growing the negative charge of the zeolite framework with cationes e.g. Ni^{2+} [32]. Carbon paste electrodes (CPEs) are preferred because of low background current, low prices and extensive potential window. Uses of improved CPEs with mesoporous materials such as zeolites have involved greatly consideration [33]. Fabrication of zeolite modified electrodes (ZMEs) is simple, fast and inexpensive that were firstly considered and encouraged by Murray et al. [34].

Electrode surfaces modification is one of the significant progresses in the latest years. $Ni(OH)_2$ is an energetic constituent in the electrochemistry because of its sharp redox presentation, high theoretical capacity and low cost [24]. According to the literature review, nanozeolite beta modified CPE was not applied for electrocatalytic oxidation of HCHO. Here, we effort to discover the influence of $Ni(OH)_2$ distributed on the nanozeolite beta modified CPE (Beta/CPE) as a novel, easy and sensitive substance for HCHO oxidation. Structure characterization of the synthesized nanozeolite beta is considered by X-ray diffraction (XRD), field emission scanning electronic microscopy (FESEM), transmission electron micrograph (TEM), Fourier transform infrared (FT-IR) and nitrogen sorption isotherms. The electrochemical performance of $Ni(OH)_2$-Beta/CPE is deliberated by cyclic voltammetry (CV), chronoamperometry, chronocoulometry and linear sweep voltammetry techniques.

2 Experimental

2.1 Reagents and materials

Tetraethyl orthosilicate (TEOS. 98%), sodium hydroxide (NaOH, 99%), tetraethylammonium hydroxide (TEAOH, 20 wt% solution in water), aluminum sulphate ($Al_2(SO_4)_3{\cdot}16H_2O$), cetyltrimethylammonium bromide (CTAB), formaldehyde, nickel chloride hexahydrate ($NiCl_2.6H_2O$), potassium hexacyanoferrate (III) ($K_3Fe(CN)_6$), potassium chloride (KCl, 99%), potassium hexacyanoferrate (II) ($K_4Fe(CN)_6$), graphite powder, and ethanol were acquired from Merck company. Paraffin oil (d = 0.88 g cm^{-3}) and diethyl ether (99 wt. %) was obtained from Daejung Company (South Korea). Furthermore, deionized water (DW) was utilized during the all experiments.

2.2 Synthesis of nanozeolite beta

Production process of nanozeolite beta have been designated in another place [31]. 27 mL of TEAOH was gradually added to 1.2 g NaOH in 4.0 mL DW. The combination was agitated for 10 minute and step up to a TEOS solution (22.3 mL) in 9.5 mL DW at 25°C and was permitted to blend for 30 minute. After it, 2.2 g of $Al_2(SO_4)_3{\cdot}16H_2O$ dissolved in 8.1 mL of DW was added to the mixture and agitated for 1 h. In the next step, 1.4 g CTAB dissolved in 40 mL ethanol and added slowly to the mixture and the gel was stirred for 2 h. The consequential viscous gel was heated at 90°C with stirring to comprehensive dryness. The dry originator lumps were obscenely rumpled and moved into a Teflon-lined autoclave. DW (ca. 0.2 mL per 1 g (dry gel)) was added into the bottom of the autoclave. The crystallization of it was performed at 175°C for 24 h. After this treatment, the powdered produces were recuperated by a runs of centrifugation at 12000 rpm and

washed with DW until pH < 8 and then dried at 25°C for 24 h. The templates were eliminated from the nanozeolite beta by calcination for 8 h at 550°C.

2.3 Apparatus and Characterization

X-ray diffraction pattern was obtained by X-ray diffractometer (XRD, MPD 3000 Instrument, Italy) with Be Filtered Cu K_{α} radiation (1.5418 Å) operating at 35.4 kV and 28.0 mA. Filed emission scanning electron microscopy (FESEM) and energy dispersive X-ray (EDX) spectroscopy were detailed by a Mira-3 XMU instrumen (Czech Republic). The Perkin Elmer Fourier transform infrared spectrometer was utilized for register of IR spectrum. Nitrogen sorption isotherms were acquired by a volumetric adsorption equipment Belsorp-max instruments, Japan. Also, a transmission electron microscope model Philips (model CM120) was used for recording of nanoparticle morphology and size. The electrochemical tests were carried out by a potentiostat/galvanostat (SAMA500 electroanalyzer system, Isfahan, Iran) with a voltammetry cell in a three electrodes configuration. The Ag|AgCl|KCl(3M) and platinum wire (from Azar Electrode Co., Iran) were utilized as reference and auxiliary electrodes. The fabricated home-made CPEs were utilized as the working electrode in the all electrochemical tests.

2.4 Fabrication of Electrode

For fabrication of Beta/CPE (25 wt.% with respect to the graphite powder), 0.05 g nanozeolite beta and 0.2 g graphite powder were carefully mixed by diethyl ether. After evaporation of diethyl ether, two drops of paraffin oil (35 wt.%) was added and combined with a mortar by hand mixing for 30 minute awaiting a regularly wetted paste was gained. This paste was crammed into the finale of a glass tube (with 4.5 mm inner diameter and 10 cm length), with a copper wire as electrical connection. A fresh surface was gotten by pushing an extra of the paste out of the tube and brush up with a weighing paper. Revision of the Beta/CPE was implemented in the two steps. Initially, the Beta/CPE was immersed in the solution of 0.1 M $NiCl_2$ for 15 min and the arranged Ni-Beta/CPE was washed by DW to eliminate adsorbed materials in the electrode surface. Then, the Ni-Beta/CPE was conditioned in 0.1 M NaOH by potential cycling in the range of 0.0 and 1.0 V for about 15 cycles at a sweep rate of 0.05 V s^{-1} for providing $Ni(OH)_2$-Beta/CPE. To obtain the operations of beta nanozeolite and $Ni(OH)_2$ in the electro-catalytic oxidation of HCHO, the $Ni(OH)_2$/CPE and Beta/CPE were prepared in similar method lacking addition the nanozeolite beta and without soaking modified electrode in the $NiCl_2$ solution, respectively.

3 Results And Discussion

3.1 Characterization of the nanozeolite beta

Figure 1(a) exhibits XRD pattern of prepared nanozeolite beta. The crystallization yields complemented the specific peaks of it with worthy crystallinity [31, 35]. The crystalline dimension of nanozeolite beta was also measured to be 33.6 nm via Debye-Scherrer equation [36]. According to the FT-IR spectrum of the nanozeolite beta in Fig. 1(b), doublet bands at 464 and 567 cm^{-1} are ascertained to the bending vibrations of Si-O or Al-O bands in β-cages, which sup\ort the existence of a zeolitic building with greatly crystallinity that is distinguishing of beta zeolite [37, 38]. The absorption band at 795 cm^{-1} is recognized to internal tetrahedral

symmetrical stretching of Si-O-Si [39]. The band positioned at 1080 cm^{-1} is ascribed to the external linkage asymmetrical stretching mode of Si-O-Si and can overlay with the Al–O–Si stretching mode [37, 40]. The band located at about 1630 cm^{-1} are ascribed to the bending vibration of H_2O adsorbed on OH^- groups [41, 42].

The BET surface area, pore diameter and pore volume of the prepared beta nanozeolite was estimated from N_2 sorption isotherm and pore size distribution investigations. Figure 1(c) displays N_2 adsorption/desorption isotherms of beta nanozeolite at 77 K that revealed H_4 type hysteresis at P/P^0 0.8-1.0 [43]. This isotherm was type-III agreeing to Brunauer arrangement and type-I according to IUPAC organization, which is a distinctive structures of microporous compounds and support the presence of great porosities in synthesized sample [44]. Figure 1(d) illustrates pore size distribution curve for nanozeolite beta was calculated as of the adsorption branches of isotherms. The textural possessions of the synthesized nanozeolite beta are specified that this substantial has great BET surface area (321 $m^2\ g^{-1}$), mean pore diameter of 1.22 nm and total pore volume (0.053 $cm^3\ g^{-1}$). This results identified that beta nanozeolite is active for adsorption of Ni ion for electrocatalytic investigation.

Transmission electron micrographs (TEM) of synthesized beta nanozeolite is demonstrated in Fig. 2(a). The TEM micrograph of it displays the agglomeration of beta nanozeolite with average particle dimension under 50 nm. Also, Fig. 2(b) demonstrates FESEM of nanozeolite beta, which specifies the foundation of semi spherical forms of beta nanozeolite by average particle size under 50 nm. These consequences indicated that particle dimension of beta nanozeolite is in settlement by gotten consequence from TEM micrograph and XRD techniques. Also, Fig. 2(c-f) exhibited elemental mapping of nanozeolite beta that specifies sodium, oxygen, silicon and aluminum elements are existed in the structure of synthesized nanozeolite beta.

3.2 FESEM and Electrochemical examination of fabricated electrodes

FESEM was done to analyze the surface arrangement of the all prepared electrodes and are illustrated in Fig. 3. As can be seen in Fig. 3(a), the layer of irregular flakes of graphite powder was presented and insulated from each other on the surface of CPE. After adding beta nanozeolite to the graphite powder for production of Beta/CPE, it can be appreciated that it was totally dispersed onto electrode surface, deducing that the beta nanozeolite was irregularly integrated into the graphite powder (Fig. 3(c)). Similarly, Figs. 3(b) and 3(d) display nickel hydroxide was wholly dispersed on the CPE and Beta/CPE surface [45].

EDX spectroscopy was assisted to obtain useful data in the existence of elements and their alignment in the structure of electrodes. The EDX spectrum and elemental mapping of $Ni(OH)_2$-Beta/CPE were presented in Fig. SM1 and the weight percent of elements in all above electrodes are accessible in Table 1. The attained data from Fig. SM1 and Table 1 represented that C, O, Na, Al, Si and Ni are existed on the $Ni(OH)_2$-Beta/CPE structure. Also, Fig. SM1 exposed homogeneous distribution of above elements in the $Ni(OH)_2$-Beta/CPE approving the identical distribution of the $Ni(OH)_2$ and beta nanozeolite in $Ni(OH)_2$-Beta/CPE structure.

Table 1
Elemental percentage (wt.%) of all fabricated electrodes extracted from EDX spectra.

Electrode	C	O	Na	Al	Si	Ni	Total
CPE	100	-	-	-	-	-	100
$Ni(OH)_2$/CPE	98.86	-	-	-	-	1.14	100
Beta/CPE	72.90	13.47	2.46	4.50	6.67	-	100
$Ni(OH)_2$-Beta/CPE	71.30	13.18	2.45	4.32	7.17	1.58	100

CVs of the bare CPE and Beta/CPE were registered in 5 mM $K_4Fe(CN)_6$ + 5 mM $K_3Fe(CN)_6$ and 0.1 M KCl solution at sweep rate 20 mV s^{-1} (display Fig. SM2(a)). The investigational consequences demonstrate reproducible anodic and cathodic peaks ascribed to the $Fe(CN)_6^{3-}/Fe(CN)_6^{4-}$ redox couple on the CPE and Beta/CPE surfaces. As can be seen, the anodic and cathodic peak current densities of Beta/CPE is greater than that at bare CPE. The variance in potential of anodic and cathodic peaks (ΔE_p) for ferricyanide was 477 mV at Beta/CPE and 400 mV at CPE. The active surface areas of the Beta/CPE and bare CPE were expected via the slope of I_{pa} vs. $\upsilon^{0.5}$ plot for a well-known concentration of $K_4Fe(CN)_6$, according to the Randles–Sevcik equation [46] (see Fig. SM2(b)). The active areas were calculated to be 1.16 and 0.14 cm^2 for Beta/CPE and bare CPE, respectively. These consequences specified that revision of CPE with nanozeolite beta causes to improve the effective surface area of the Beta/CPE.

3.3 Electrocatalytic oxidation of HCHO

Figure 4 demonstrates CVs of bare CPE, Beta/CPE, $Ni(OH)_2$/CPE and $Ni(OH)_2$-Beta/CPE in 0.1 M NaOH solution at the potential range of 0.1–0.8 V vs. Ag|AgCl|KCl (3M) at sweep rate of 20 mV s^{-1} without and with HCHO. According to the Fig. 4(a) and 4(b), no redox peak can be detected on the CPE and Beta/CPE surfaces which ascends from high overpotential for HCHO electrooxidation at these electrodes and the existence of a kinetically sluggish oxidation procedure [26]. Also, the background current for Beta/CPE is greater than that on bare CPE because of greater surface area of nanozeolite beta in the structure of Beta/CPE [44, 47].

Presence of Ni^{2+} at the fabricated electrodes were considered by CVs comparison of $Ni(OH)_2$-Beta/CPE and $Ni(OH)_2$/CPE without and with 20 mM HCHO (see Figs. 4(c) and 4(d)). In the absence of HCHO, a couple of well-identified redox peaks with great oxidation peak current density (j_{pa} = 1.97 mA cm^{-2}) and ΔE_p of 180 mV can be distinguished on $Ni(OH)_2$-Beta/CPE (see Fig. 4(d)). But, the redox peaks with weak anodic signal (j_{pa} = 0.15 mA cm^{-2}) was appeared on bare CPE with ΔE_p of 120 mV (see Fig. 4(c)). Since the active microscopic area of Beta/CPE is about 8.3-fold bigger than that at bare CPE, accumulation of Ni^{2+} and achieved oxidation currents on Beta/CPE are larger than that on the bare CPE. It can be deduced that the existence of nanozeolite beta in the structure of fabricated CPE had an excessive influence on the improvement of the oxidation current densities for $Ni(OH)_2$ to Ni(OOH) conversion (see Fig. 4(e)). It is proposed that at the interface of Ni(II)-Beta/CPE and electrolyte in 0.1 M NaOH, Ni^{2+} react with OH^- to generate $Ni(OH)_2$-Beta/CPE that doings as active location in the redox procedure. In the lack of HCHO in Fig. 4(d), the anodic peak related to the

oxidation of $Ni(OH)_2$-Beta/CPE to Ni(OOH)-Beta/CPE, and the cathodic peak ascribed to the inverse transformation [48–51].

To distinguish the influence of nanozeolite beta, the CVs of CPE, Beta/CPE, $Ni(OH)_2$/CPE, and $Ni(OH)_2$-Beta/CPE were displayed in the existence of 20 mM HCHO in Fig. 4(f). According to this Fig., no anodic currents were observed for electro-oxidation of HCHO on the CPE and Beta/CPE surfaces. A small anodic peak was detected around 0.52 V on $Ni(OH)_2$/CPE that is specialized to HCHO oxidation in the existence of little $Ni(OH)_2$ on the bare CPE. This statement specifies little affinity of graphite to the adsorption of Ni^{2+}. Diffusion of Ni^{2+} ions in nanozeolite beta is greatly more rapidly because of Ni^{2+} coordination to the nanozeolite framework, the larger cages and channels and fast movement of Ni^{2+} ions from the cages [26, 42]. Also, the broad cathodic peak in some plots in Fig. 4 might be ascribed to the phase conversion of β-NiOOH to γ-NiOOH because of sluggish, irreversible over-charging for the period of cycling, and the matching reduction to α-$Ni(OH)_2$ [52]. Meanwhile, catalytic current of HCHO electro-oxidation onto $Ni(OH)_2$-Beta/CPE is more larger than that obtained on the $Ni(OH)_2$/CPE. The greater presentation of $Ni(OH)_2$-Beta/CPE for electro-oxidation of HCHO can be accredited to the existence of mesoporous nanozeolite beta in the composition of Beta/CPE that improve electro-active surface area of modified CPE.

The enhancement in anodic peak current was detected on $Ni(OH)_2$-Beta/CPE at 0.61 V and the cathodic peak current at about 0.28 V was reduced in the existence of HCHO (see Fig. 4(d)). This consequence identified that employed nanozeolite beta as modifier in this procedure contributes straightly in the HCHO electro-oxidation. Captivating into explanation, all these explanations were in agreement by the previous works [25, 50, 53, 54] and we might mentioned a mechanism for electro-catalytic oxidation of HCHO on the $Ni(OH)_2$-Beta/CPE surface. In aqueous solution, the HCHO is totally hydrated and changed to the methylene glycol ($CH_2(OH)_2$) by an equilibrium constant of 2.28×10^3. Because of its pK_a (ca. 12.8), the $CH_2(OH)_2$ occurs generally in its ionized stat ($CH_2(OH)O^-$) in alkaline solution [55, 56]. When $CH_2(OH)O^-$ diffuses from the bulk solution to the surface of modified electrode, it is speedily oxidized to $CH_2(O)O^-$ by the NiOOH molecules on the surface of $Ni(OH)_2$-Beta/CPE. Consequently, the quantity of NiOOH reduced because of its chemical reaction with $CH_2(OH)O^-$. In the complete reaction, HCHO can be altered to the $CH_2(O)O^-$ ion and produced one electron. Basically, this mechanism is a characteristic appreciation predicted from the mediated oxidation (electro-catalytic reaction, EC' mechanism) [5, 25, 50, 53, 57]. The electrocatalytic oxidation mechanism for HCHO on $Ni(OH)_2$-Beta/CPE might be defined by the next equations:

$$\mathrm{HCHO + H_2O \rightleftarrows CH_2(OH)_2 K_{eq} = 2.28 \times 10^3} (1)$$

$$\mathrm{CH_2(OH)_2 + OH^- \rightleftarrows CH_2(OH)O^- + H_2O} (2)$$

\left[\left({\text{N}\text{i}\left(\text{O}\text{H}\right)}_{2}-\text{B}\text{e}\text{t}\text{a}/\text{C}\text{P}\text{E}\right)\right]+{\text{O}\text{H}}^{-}\rightleftarrows \left[\left(\text{N}\text{i}\text{O}\text{O}\text{H}-\text{B}\text{e}\text{t}\text{a}/\text{C}\text{P}\text{E} \right)\right] +{\text{H}}_{2}\text{O}+ {\text{e}}^{-} \left(3\right)

\left[\left(\text{N}\text{i}\text{O}\text{O}\text{H}-\text{B}\text{e}\text{t}\text{a}/\text{C}\text{P}\text{E}\right)\right]+\text{C}{\text{H}}_{2}\left(\text{O}\text{H}\right){\text{O}}^{-} \to \left[\left({\text{N}\text{i}\left(\text{O}\text{H}\right)}_{2}-\text{B}\text{e}\text{t}\text{a}/\text{C}\text{P}\text{E}\right)\right]+\text{C}{\text{H}}_{2}\left(\text{O}\right){\text{O}}^{-} \left(4\right)

It was commonly accepted that NiOOH in the surface of modified electrode at 0.1 M NaOH catalyze the oxidation of HCHO through one electron procedure for generating format anions as ending produce [5, 57]. The sum of the above equations could be stated as below:

\text{H}\text{C}\text{H}\text{O}+ {2 \text{O}\text{H}}^{-}\rightleftarrows \text{C}{\text{H}}_{2}\left(\text{O}\right){\text{O}}^{-} {\text{H}}_{2}\text{O}+{\text{e}}^{-} \left(5\right)

Prepared electrodes at different ratio of 15, 25 and 40% wt./wt. vs. graphite were considered by CV technique. It was detected that the ratio of 25% nanozeolite beta in the fabricated electrode has maximum anodic current for electro-oxidation of HCHO. In 15% wt./wt. of nanozeolite beta in CPE, the low accessible pores of the nanozeolite for Ni^{2+} loading and in 40% wt./wt. more resistance of modified electrode because of nonconductive characteristic of nanozeolite beta are chief aspects which origin to reduce anodic current densities [26].

3.4 Effect of sweep rate without and with HCHO

Influence of sweep rate was considered on the redox performance of $Ni(OH)_2$-Beta/CPE without HCHO in 0.1 M NaOH solution and are shown in Fig. SM3(a). A couple of well-formed redox peaks by a ΔE_p of 170 mV is identified at sweep rate of 10 mV s^{-1}. The ΔE_p growths with improving sweep rate that specifies the attendance of a inadequacy in charge transfer kinetics [58]. At $\Delta E_p > 0.2/n$ V from a theory described by Laviron [59], we can be estimated the electron transfer coefficient (α) by calculating the alteration of the peak potential (E_p) vs. log υ and apparent charge transfer rate constant (k_s). Fig. SM3(b) displays the curve of E_p vs. log υ in 5-600 mV s^{-1} for cathodic and anodic peaks. It can be appreciated that E_p is proportionate to log υ at $\upsilon >$ 100 mV s^{-1} definite by Laviron [59]. The quantity of α is obtained to be 0.52 signifying speed limiting stages for cathodic and anodic can be nearly the identical step [60]. The average quantity of k_s over this range of sweep rate is obtained to be 0.043 s^{-1}. In relation to the slope of two lines in Fig. SM3(c), the surface coverage of the $Ni(OH)_2$/Ni(OOH on $Ni(OH)_2$-Beta/CPE can be expected to be 2.3×10^{-8} mol cm^{-2} [61]. The quantity of loaded Ni on the modified electrode surface is achieved to be 0.215 µg. At great sweep rates in Fig. SM3(d), the peak current densities are proportionate to $\upsilon^{0.5}$, indicating to the freely diffusion controlled process [62, 63].

CVs of the $Ni(OH)_2$-Beta/CPE in the existence of 22 mM HCHO at different sweep rates (5-600 mV s^{-1}) in 0.1 M NaOH were displayed in Fig. 5(a). As the sweep rate growths, the anodic peak current for HCHO oxidation improves. The remaining cathodic peak ascertained for reduction of the residual NiOOH to $Ni(OH)_2$ increases by sweep rate. This may because of the statement that the persisted NiOOH increases with growing the sweep rate because of lower consumption of the NiOOH at greater sweep rates [5]. A curve of j_{pa} vs. υ did not display a linear plot (Fig. 5(b)); meanwhile, curve of j_{pa} against $\upsilon^{0.5}$ was establish to be linear (see Fig. 5(c)).

This item suggested that this procedure is diffusion controlled procedure instead of surface controlled process [64].

A straight line is attained (R^2 = 0.9974) which is in agreement by the Randles-Sevcik equation for totally irreversible diffusion-controlled procedure and specified by the following equation [61]:

{\text{I}}_{\text{p}}= 0.4961 \text{n}\text{F}\text{A}\text{C}{\left(\frac{{\alpha }{\text{n}}_{{\alpha }}\text{F}\text{D}}{\text{R}\text{T}}\right)}^{0.5}{\upsilon }^{0.5} \left(6\right)

where I_p pointed to the anodic peak current (A), A is the surface area of the modified electrode (cm^2), D is the diffusion coefficient of HCHO ($cm^2\ s^{-1}$), n is the total number of electrons (e.g. 1), C is the bulk concentration of HCHO (mol cm^{-3}) and υ is the sweep rate (V s^{-1}). Also, α is the charge transfer coefficient, n_α is the number of electrons in the rate determining stage, F is the Faraday's constant (96485 C mol^{-1}), R is the gas constant (8.314 J $mol^{-1}\ K^{-1}$) and T is the absolute temperature (298 K). The amount of an_α can be measured using the following equation [65]:

{|\text{E}}_{\text{p}}- {\text{E}}_{\text{p}/2}|= \frac{1.857 \text{R}\text{T}}{{\alpha }{\text{n}}_{{\alpha }}\text{F}} (7)

where E_p is the peak potential and $E_{p/2}$ is the potential at half peak current. The information in Fig. 5(a) was utilized to estimate the parameter an_α at various sweep rates. The mean value was obtained to be 0.344. It can be stated that this amount is fewer than that found in the blank that may argument to some kinetic limitations in the existence of the HCHO because of probable poisoning of the modified electrode surface with the oxidation produces. From Eq. (6), slope of the straight line in the inset of Fig. 5(c) and the amount of an_α (i.e. 0.344) the D value was calculate to be 2.97×10^{-7} $cm^2\ s^{-1}$.

A linear segment is detected on the curve of log j_{pa} vs. log υ by slope of 0.2976 (see Fig. 5(d)) which is nearly the theoretically estimated value of 0.5 for a justly diffusion-controlled process. Small alteration by theoretical amount rises possibly from kinetic limitation in the total reaction [46]. A polynomial decrease in curve of normalized current density ($j_{pa}/\upsilon^{0.5}$) versus υ in Fig. 5(e), describes an EC' procedure and highlight that an irreversible continuation chemical stage is elaborate in the total procedure [66, 67]. Influence of sweep rate on the proportion of anodic to cathodic current without and with HCHO was exhibited in Fig. 5(f). This Fig. demonstrates that the I_{pa}/I_{pc} in the existence of HCHO was reduced meaningfully by growing sweep rate. Consequently, drop in the period for HCHO oxidation at greater sweep rates abstained the superficial electron transfer between NiOOH and HCHO molecule [57].

The linear sweep voltammograms (LSVs) of the $Ni(OH)_2$-Beta/CPE in 0.1 M NaOH solution including 22 mM HCHO shown in Fig. SM4(a) at sweep rates of 0.003, 0.005, 0.007 and 0.010 V s^{-1}. Fig. SM4(b) displays the Tafel plots (log I vs. E) strained from the data resulting by the growing portion of the current voltage curves. This raising section of voltammogram, identified as Tafel region, is influenced by electron transfer kinetics between the HCHO and $Ni(OH)_2$-Beta/CPE. The Tafel slope is identical to $n(1-\alpha)F/2.303RT$, where n is number of electron in the rate measuring stage (i. e. $n = 1$) and α, F, R and T have their common meaning.

According to the above declared quasi reversible electron transfer kinetics and Tafel slope for four curves, the quantity of α was achieved to be 0.69 presuming a one electron developed in the rate measuring stage [68, 69].

3.5 Effect of HCHO concentration

Figures 6(a) and 6(b) exhibit CVs of $Ni(OH)_2$-Beta/CPE at different concentration of HCHO. As can be detected that the anodic peak current improved by growing HCHO concentration. It can be identified that upon growing HCHO concentration, the onset potential of the $Ni(OH)_2$ oxidation motivated to positive values. This is maybe because of the adsorption of intermediates on the residual active locations that obstruct the additional HCHO oxidation and then, more overpotential is needed for HCHO oxidation. Plot of the current density versus HCHO is represented in Fig. 6(c) that contained of 2 linear sections in the concentration ranges of 0 to 20 mM and 20 to 140 mM. At higher concentration range (20–140 mM), adsorption of the oxidation produces at $Ni(OH)_2$-Beta/CPE may reason the discontinuation of further oxidation and then, slope of calibration curve was decreased [46, 70]. The curve of normalized current voltammogram at $Ni(OH)_2$-Beta/CPE is exhibited in the Fig. 6(d). The value of inserted Ni^{2+} is obtained from the surface coverage.

3.6 Chronoamperometric and chronocoulometric studies

Some chronoamperometric and chronocoulometric readings were accomplished to estimate the electro-catalytic management of the $Ni(OH)_2$-Beta/CPE for HCHO. Figure 7(a) displays chronoamperograms of redox process registered by location the potential of $Ni(OH)_2$-Beta/CPE at 0.65 and 0.25 V vs. Ag|AgCl|KCl(3M) without and with various HCHO concentrations. It was detected that attained currents from these tests were in worthy arrangement by the achieved date from CV experiments and the current densities progress as the HCHO concentration growths. This consequence confirms our deduction in the case of the catalytic character of NiOOH for HCHO oxidation on the $Ni(OH)_2$-Beta/CPE surface [71].

For an electro-active compound by a diffusion process, the practical current for the electrochemical reaction underneath mass transportation limited situations can be stated with the Cottrell equation [72]:

\text{I} =\text{n}\text{F}\text{A}\text{C}{\text{D}}^{0.5}{{\pi }}^{-0.5}{\text{t}}^{-0.5} \left(8\right)

where n is the number of electron (i.e., 1), A is the area of the electrode (0.159 cm^2) and F, C and D have their common meaning. Practical curves of I versus $t^{-0.5}$ for all HCHO concentrations were plotted and the best fits for different HCHO concentrations were obtained (Fig. 7(b)). The slopes of the consequential lines were plotted against three concentrations of HCHO and was displayed in Fig. 7(c). From the obtained slope and Eq. (8), the average quantity of D was gotten to be 4.4×10^{-7} cm^2 s^{-1}. This amount is comparable with the value estimated from Eq. (6).

The chronoamperometry technique can be employed for the assessment of the catalytic rate constant (k_{cat}) of an analyte on the active positions of the fabricated $Ni(OH)_2$-Beta/CPE rendering to the next equation [73]:

\frac{{I}_{cat}}{{I}_{L}}={\left({\pi }{k}_{cat}{C}_{0}\right)}^{0.5} {t}^{0.5} \left(9\right)

where, I_{cat} and I_L are the currents without and with HCHO, respectively. The C_0 is the bulk concentration of HCHO (mol cm^{-3}) and t is the elapsed time (second). using the slopes of I_{cat}/I_L against $t^{0.5}$ (Fig. 7(d)) for all concentrations, the average value of k_{cat} was estimated to be 2.08×10^6 cm^3 mol^{-1} s^{-1}. Judgment of the expected k_{cat} in this work by others in the earliest papers is done and exhibited in Table 2. According to this Table, the $Ni(OH)_2$-Beta/CPE can act as a comparable catalyst in HCHO electro-catalytic oxidation. Also, j_{pa} and E_{pa} were compared for HCHO electro-catalytic oxidation at the surface of modified electrode by several previous papers. According to this table, j_{pa} with $Ni(OH)_2$-Beta/CPE is greater than that on the some of the earlier works.

Table 2
Comparison of the electro-catalytic activity of the $Ni(OH)_2$-Beta/CPE for HCHO oxidation with some of the Ni modified electrodes.

Electrode	HCHO Concentration	Sweep rate / mV s^{-1}	j_{pa} / mA cm^{-2}	E_p vs. Ag|AgCl| KCl(3M) / V	pH	E_p vs. RHE / V	k_{cat} / cm^3 mol^{-1} s^{-1}	Ref.
Nano-NiPh/GCE[a]	0.005 M	20	3.5	0.7	13.0	1.67	4.0×10^6	[5]
Ni-Pd/GCE	0.01 M	50	6.8	0.52	13.7	1.53	—	[20]
$Ni(OH)_2$-MIL/CPE[b]	0.015 M	20	6.5	0.60	13.0	1.57	2.37×10^2	[24]
Ni-P/CPE[c]	0.035 M	25	12	0.70	13.0	1.67	1.7×10^4	[25]
Ni/ANA/CPE[d]	0.03 M	20	4.2	0.62	13.0	1.59	7.56×10^4	[26]
$Ni(OH)_2$-X/CPE[e]	0.1 M	50	24.8	0.67	13.0	1.64	6.1×10^4	[28]
Ni-CoVSB-5/CPE[f]	0.01 M	20	3.2	0.60	13.0	1.57	1.80×10^5	[50]
Ni-HTN/CPE[g]	0.02 M	25	2.9	0.62	13.0	1.59	2.65×10^4	[51]
Ni/IL/CPE[h]	0.1 M	20	16.5	0.71	13.0	1.68	1.58×10^6	[57]
NiNPs/ITO[k]	0.1 M	100	1.6	0.68	13.0	1.65	—	[74]
Ni/P(1,5-DAN)/MCPE[l]	0.1 M	10	0.76	0.80	13.0	1.77	2×10^6	[75]
$Ni(OH)_2$/POT (TX-100) /CNTPE[m]	0.048 M	20	12.1	0.70	13.0	1.67	1.1×10^5	[76]
Ni/P(NMA)/MCPE[n]	0.07 M	20	4.1	0.74	13.0	1.71	8.96×10^4	[77]
$Ni(OH)_2$-Beta/CP\E[o]	0.02 M	20	1.97	0.61	13.0	1.58	2.08×10^6	Present study

[a] Nano-NiPh/GCE: Nanoporous nickel phosphate/glassy carbon electrode

[b] $Ni(OH)_2$-MIL/CPE: Nickel hydroxide-MIL-101(Cr) MOF nanoparticle/carbon paste electrode

[c] Ni-P/CPE: Nickel-P nanozeolite/carbon paste electrode

[d] Ni/ANA/CPE: Nickel/analcime nanozeolite/carbon paste electrode

[e] $Ni(OH)_2$-X/CPE: Nickel hydroxide-NaX nanozeolite/carbon paste electrode

[f] Ni-CoVSB-5/CPE: Nickel-cobalt Versailles Santa Barbara-5/carbon paste electrode

Electrode	HCHO Concentration	Sweep rate / mV s^{-1}	j_{pa} / mA cm^{-2}	E_p vs. Ag|AgCl| KCl(3M) / V	pH	E_p vs. RHE / V	k_{cat} / cm^3 mol^{-1} s^{-1}	Ref.
[g] Ni-HTN/CPE: Nickel-hydrogen titanate nanotubes/carbon paste electrode								
[h] Ni/IL/CPE: Nickel/ionic liquid/carbon paste electrode								
[k] NiNPs/ITO: Nickel nanoparticles/indium tin oxide electrode								
[l] Ni/P(1,5-DAN)/MCPE: Nickel/poly (1,5-diaminonaphthalene)/modified carbon paste electrode								
[m] $Ni(OH)_2$/POT (TX-100)/CNTPE: Nickel hydroxide /poly (o-toluidine)/Triton X-100/carbon nanotube paste electrode								
[n] Ni/P(NMA)/MCPE: Nickel/ Poly (N-methylaniline)/modified carbon paste electrode								
[o] $Ni(OH)_2$-Beta/CPE : Nickel hydroxide-nanozeolite Beta/carbon paste electrode								

The HCHO electro-oxidation on the $Ni(OH)_2$-Beta/CPE surface was studied by chronocoulometry method. Figure 8(a) displays the double steps chronocoulomograms without and with various HCHO concentration (30–140 mM) with potential stages of 0.65 and 0.25 V. The chronocoulometric plot of $Ni(OH)_2$-Beta/CPE in the 0.1 M NaOH displayed an practically symmetrical form. It can be deduced that nearly same charges were consumed for the oxidation and reduction of $Ni(OH)_2$/NiOOH in the surface of modified electrode. In the existence of HCHO, the charge amount related to the advancing chronocoulometry is larger than that detected on backward chronocoulometry. The charge quantity attendant with the backward chronocoulometry is generally decreased by growth in HCHO concentration demonstrating that the electro-catalytic oxidation procedures are irreversible [61, 67]. This consequence discovered a like performance to those defined by CV technique.

Also, chronocoulometry method was also applied to estimate the *D* of HCHO in the modified CPE surface. The charge answer under diffusion-controled is designated using the next equation [61, 67]:

\text{Q} =2\text{n}\text{F}\text{A}\text{C}{\text{D}}^{0.5}.{{\pi }}^{-0.5}{.\text{t}}^{0.5} \left(10\right)

For estimate of the *D*, Fig. 8(b) was displayed curves of *Q* vs. $t^{0.5}$ for all HCHO concentrations at $Ni(OH)_2$-Beta/CPE surface. In the next step, the slopes of the resultant straight lines was planned versus HCHO concentration (see Fig. 8(c)). From the slope of the subsequent plots and applying Eq. (10), the average quantity of *D* was obtained to be 2.13×10^{-6} cm^2 s^{-1} in the HCHO concentration scale of 30–140 mM.

3.7 Stability, repeatability and reproducibility of the $Ni(OH)_2$-Beta/CPE

For a fresh method, long-term stability is a substantial parameter. It was considered with captivating the answer of $Ni(OH)_2$-Beta/CPE in three months. The $Ni(OH)_2$-Beta/CPE was reserved in open air at temperature of 298 K while not in custom. The gained answers were considered with analysis of variance (ANOVA) test. The F_{exp} (i.e. 3.4) matched to its critical quantity at 95% confidence level ($F_{0.05,5,5}$ = 4.95). It can be indicated that deviances among the modified electrode answers are because of random errors and the electrode memorized its complete action through this time. It was important to progress the surface by a slight rubbing of the modified CPE on a soft paper, at any time the electrode answer decreased. Also, the $Ni(OH)_2$-Beta/CPE was introduced to fifty cycles with the sweep rate of 50 mV s^{-1} in 0.1 M NaOH without and with 20 mM HCHO (see Figs. 8(d) and 8(e)). This electrode reserved 96.4 and 90.1% of its primary current answer after 50 repetitive cycles without and with HCHO, respectively. No important variation was revealed in the potential of anodic peak at two Figs. These consequences specify mechanical and chemical stability and reproducible answer as well as long-term stability of the $Ni(OH)_2$-Beta/CPE for HCHO electro-catalytic oxidation [58].

The reproducibility of the $Ni(OH)_2$-Beta/CPE was evaluated through the comparison of the currents of 4 various modified electrodes comprising 25 wt.% of nanozeolite beta by CV technique. The oxidation current density of these electrodes for electro-oxidation of 20 mM HCHO was considered individually and the RSD was 3.45%. A reproducible current answer with a RSD of 3.12% was detected for 4 consecutive assays of 20 mM HCHO. For additional consideration of the electro activity and long term stability of the catalysts, cronoamperograms at potential of 0.65 V were registered for the $Ni(OH)_2$-Beta/CPE and $Ni(OH)_2$/CPE in 0.1 M NaOH and 20 mM HCHO (see Fig. 8(f)). Accordance to this Fig., a reduce in current by time is obtained in order of $Ni(OH)_2$-Beta/CPE > $Ni(OH)_2$/CPE, that is in worthy covenant with the CV information. These outcomes indicated that the $Ni(OH)_2$-Beta/CPE has superior poisoning tolerance capacity for HCHO oxidation and is a better electrode for long term process. As can be understood, the reduce in current at first times is reasonably great for modified electrode. However, the current reaches a moderately stable quantity when the time is above 60 s demonstrating that $Ni(OH)_2$-Beta/CPE displays An acceptable stability for HCHO oxidation [42]. Also, nanozeolite beta was stayed stable in the building of modified electrode at 0.1 M NaOH [78].

4 Conclusions

In this paper, nanozeolite beta was synthesized using simple hydrothermal process and was characterized by different methods containing XRD, FTIR, FESEM, TEM and N_2 sorption techniques. The role of synthesized sample in the HCHO electro-oxidation was estimated by preparation of modified CPEs including nanozeolite beta and $Ni(OH)_2$ by cyclic voltammetry, chronocoulometry, chronoamperometry and linear sweep voltammetry methods. It was obtained that nanozeolite beta as porous material by good BET surface area and large number of active locations performs as host for adsorption of Ni^{2+} and NiOOH produced throughout the oxidation of $Ni(OH)_2$ in the 0.1 M NaOH solution. The consequences demonstrate that $Ni(OH)_2$-Beta/CPE can increase the HCHO oxidation by a catalytic procedure via a reduce in overpotential and overawed the low kinetic of reaction in confronting with $Ni(OH)_2$/CPE and some of the previous works. Some significant kinetic and transport parameters were calculated and compared by those in literatures. As an example, the diffusion coefficient and catalytic rate constant of HCHO are achieved to be 2.13×10^{-6} cm^2 s^{-1} and 2.08×10^6 cm^3 mol^{-1} s^{-1} by chronocoulometry and chronoamperometry, respectively. Also, the stability

and presentation of the $Ni(OH)_2$-Beta/CPE was investigated at the experimental conditions. The CV test specified that the current density of HCHO electro-oxidation improves strangely on $Ni(OH)_2$-Beta/CPE. It reserves that nanozeolite beta has an excellent support for $Ni(OH)_2$ and attending it as operational catalysts for HCHO electro-catalytic oxidation could cause new prospects for fuel cell technology.

Declarations

Acknowledgements

We are grateful for financial support from the Research Council of Babol Noshirvani University of Technology.

Funding information

The authors state that there has no funding information.

Declaration of competing interest

The authors declare that there has no conflict of interest.

References

1. B. Yang, et al., Solution plasma method for the preparation of Cu-Ni/CuO-NiO with excellent methanol electrocatalytic oxidation performance. Appl. Surf. Sci. **513**, 145808 (2020)

2. H.S. Ferreira, et al., Improved electrocatalytic activity of Pt supported onto Fe-doped TiO2 toward ethanol oxidation in acid media. Mater. Chem. Phys. **245**, 122753 (2020)

3. I. Pötzelberger, et al., Maximum electrocatalytic oxidation performance for formaldehyde in a combinatorial copper-palladium thin film library. Appl. Catal. A-Gen. **525**, 110-118 (2016)

4. S.R. Hosseini, et al., Pd-Cu/poly (o-Anisidine) nanocomposite as an efficient catalyst for formaldehyde oxidation. Mater. Res. Bull. **80**, 107-119 (2016)

5. A. Touny, R.H. Tammam, and M. Saleh, Electrocatalytic oxidation of formaldehyde on nanoporous nickel phosphate modified electrode. Appl. Catal. B-Environ. **224**, 1017-1026 (2018)

6. R. Ojani, et al., Copper-poly (2-aminodiphenylamine) composite as catalyst for electrocatalytic oxidation of formaldehyde in alkaline media. Int. J. Hydrogen Energy, **38**, 5457-5463 (2013)

7. C. Korzeniewski and C.L. Childers, Formaldehyde yields from methanol electrochemical oxidation on platinum. J. Phys. Chem. B, **102**, 489-492 (1998)

8. S.K. Hassaninejad–Darzi, A novel, effective and low cost catalyst for formaldehyde electrooxidation based on nickel ions dispersed onto chitosan-modified carbon paste electrode for fuel cell. J. Electroceram. **33**, 252-263 (2014)

9. A. Safavi, et al., Electrocatalytic oxidation of formaldehyde on palladium nanoparticles electrodeposited on carbon ionic liquid composite electrode. J. Electroanal. Chem. **626**, 75-79 (2009)

10. C. Zhang, et al., Synthesis of MnO2 modified porous carbon spheres by preoxidation-assisted impregnation for catalytic oxidation of indoor formaldehyde. J. Porous Mater. **27**, 801-815 (2020)

11. Y. Xia, et al., Preparation of high surface area mesoporous nickel oxides and catalytic oxidation of toluene and formaldehyde. J. Porous Mater. **24**, 621-629 (2017)

12. F. Niu and Q. Yi, A novel nanoporous palladium catalyst for formaldehyde electro-oxidation in alkaline media. Rare Metals, **30**, 102-105 (2011)

13. J.-B. Raoof, S.R. Hosseini, and S. Rezaee, A simple and effective route for preparation of platinum nanoparticle and its application for electrocatalytic oxidation of methanol and formaldehyde. J. Mol. Liq. **212**, 767-774 (2015)

14. B. Habibi and S. Ghaderi, Electrooxidation of Formic Acid and Formaldehyde on the Fe3O4@ Pt Core-Shell Nanoparticles/Carbon-Ceramic Electrode. Iran. J. Chem. Chem. Eng. **35**, 99-112 (2016)

15. Y. Chen, et al., Enhanced formaldehyde oxidation on Pt/MnO2 catalysts modified with alkali metal salts. J. Colloid Interface Sci. **428**, 1-7 (2014)

16. J.-B. Raoof, et al., Fabrication of bimetallic Cu/Pd particles modified carbon nanotube paste electrode and its use towards formaldehyde electrooxidation. J. Mol. Liq. **204**, 106-111 (2015)

17. V. Selvaraj, A.N. Grace, and M. Alagar, Electrocatalytic oxidation of formic acid and formaldehyde on nanoparticle decorated single walled carbon nanotubes. J. Colloid Interface Sci. **333**, 254-262 (2009)

18. J. Monzó, et al., Electrochemical oxidation of small organic molecules on Au nanoparticles with preferential surface orientation. ChemElectroChem, **2**, 958-962 (2015)

19. G. Padmalaya, et al., Synthesis of Micro-dumbbell Shaped rGO/ZnO Composite Rods and Its Application Towards as Electrochemical Sensor for the Simultaneous Determination of Ammonia and Formaldehyde Using Hexamine and Its Structural Analysis. J. Inorg. Organomet. P. **30**, 943-954 (2020)

20. E.O. Nachaki, et al., Nickel-Palladium-Based Electrochemical Sensor for Quantitative Detection of Formaldehyde. ChemistrySelect. **3**, 384-392 (2018)

21. S.A. Al-Jendan, et al., An optimized nickel phosphate/carbon composite electrocatalyst for the oxidation of formaldehyde. Int. J. Hydrogen Energy, **45**, 14320-14333 (2020)

22. Š. Trafela, S. Šturm, and K.Ž. Rožman, Surface modification for the enhanced electrocatalytic HCHO oxidation performance of Ni-thin-film-based catalysts. Appl. Surf. Sci. **537**, 147822 (2021)

23. T. Yang, et al., Efficient formaldehyde oxidation over nickel hydroxide promoted Pt/γ-Al 2 O 3 with a low Pt content. Appl. Catal. B-Environ. **200**, 543-551 (2017)

24. S. Gheytani, S. Hassaninejad-Darzi, and M. Taherimehr, Formaldehyde Electro-catalytic Oxidation onto Carbon Paste Electrode Modified by MIL-101 (Cr) Nanoparticles. Fuel Cells, **20**, 3-16 (2020)

25. S.N. Azizi, S. Ghasemi, and F. Amiripour, Nickel/P nanozeolite modified electrode: a new sensor for the detection of formaldehyde. Sensors Actuators B: Chem. **227**, 1-10 (2016)

26. S.N. Azizi, S. Ghasemi, and M. Derakhshani-mansoorkuhi, The synthesis of analcime zeolite nanoparticles using silica extracted from stem of sorghum Halepenesic ash and their application as support for electrooxidation of formaldehyde. Int. J. Hydrogen Energy, **41**, 21181-21192 (2016)

27. S. Hassaninejad-Darzi, M. Rahimnejad, and M. Gholami-Esfidvajani, Electrocatalytic Oxidation of Formaldehyde onto Carbon Paste Electrode Modified with Nickel Decorated Nanoporous Cobalt-Nickel Phosphate Molecular Sieve for Fuel Cell. Fuel Cells, **16**, 89-99 (2016)

28. S. Kavian, S.N. Azizi, and S. Ghasemi, Preparation of a novel supported electrode comprising a nickel (II) hydroxide-modified carbon paste electrode (Ni (OH) 2-X/CPE) for the electrocatalytic oxidation of formaldehyde. Chinese J. Catal. **37**, 159-168 (2016)

29. M. Abrishamkar and F.B. Kahkeshi, Synthesis and characterization of nano-ZSM-5 zeolite and its application for electrocatalytic oxidation of formaldehyde over modified carbon paste electrode with ion exchanged synthesized zeolite in alkaline media. Micropor. Mesopor. Mater. **167**, 51-54 (2013)

30. J.B. Raoof, et al., Ni/ZSM-5 Zeolite Modified Carbon Paste Electrode as an Efficient Electrode for Electrocatalytic Oxidation of Formaldehyde. J. Chin. Chem. Soc. **60**, 546-550 (2013)

31. M.M. Reddy, et al., N-Alkylation of amines with alcohols over nanosized zeolite beta. Green Chem. **15**, 3474-3483 (2013)

32. S. Mintova, et al., Variation of the Si/Al ratio in nanosized zeolite Beta crystals. Micropor. Mesopor. Mater. **90**, 237-245 (2006)

33. B.M. Daas and S. Ghosh, Fuel cell applications of chemically synthesized zeolite modified electrode (ZME) as catalyst for alcohol electro-oxidation-A review. J. Electroanal. Chem. **783**, 308-315 (2016)

34. R.W. Murray, A.G. Ewing, and R.A. Durst, Chemically modified electrodes. Molecular design for electroanalysis. Anal. Chem. **59**, 379A-390A (1987)

35. M.M. Treacy and J.B. Higgins, *Collection of Simulated XRD Powder Patterns for Zeolites Fifth (5th) Revised Edition*. (Elsevier, 2007)

36. N.B. Castagnola and P.K. Dutta, Nanometer-sized zeolite X crystals: Use as photochemical hosts. The J. Phys. Chem. B, **102**, 1696-1702 (1998)

37. N. Goyal, V.K. Bulasara, and S. Barman, Removal of emerging contaminants daidzein and coumestrol from water by nanozeolite beta modified with tetrasubstituted ammonium cation. J. Hazard. Mater. **344**, 417-430 (2018)

38. B. Schoeman, et al., The synthesis of discrete colloidal crystals of zeolite beta and their application in the preparation of thin microporous films. J. Porous Mater. **8**, 13-22 (2001)

39. G. Huang, et al., Fast synthesis of hierarchical Beta zeolites with uniform nanocrystals from layered silicate precursor. Micropor. Mesopor. Mater. **248**, 30-39 (2017)

40. Q. Lin, et al., Electrocatalytic oxidation of ethylene glycol and glycerol on nickel ion implanted-modified indium tin oxide electrode. Int. J. Hydrogen Energy, **42**, 1403-1411 (2017)

41. S.K. Hassaninejad–Darzi, M. Rahimnejad, and S.N. Mirzababaei, Electrocatalytic oxidation of glucose onto carbon paste electrode modified with nickel hydroxide decorated NaA nanozeolite. Microchem. J. **128**, 7-17 (2016)

42. S. Eshagh-Nimvari and S. Karim Hassaninejad-Darzi, Synergistic effects of nanozeolite beta-MWCNTs on the electrocatalytic oxidation of ethylene glycol: Experimental design by response surface methodology. Mater. Sci. Eng.-B, **268**, 115125 (2021)

43. K.S. Sing, Reporting physisorption data for gas/solid systems with special reference to the determination of surface area and porosity (Recommendations 1984). Pure Appl. Chem. **57**, 603-619 (1985)

44. B. Aghamohseni, S.K. Hassaninejad-Darzi, and M. Asadollahi-Baboli, A new sensitive voltammetric determination of thymol based on MnY nanozeolite modified carbon paste electrode using response surface methodology. Microchem. J. **145**, 819-832 (2019)

45. S.K. Hassaninejad-Darzi and M. Gholami-Esfidvajani, Electrocatalytic oxidation of ethanol using modified nickel phosphate nanoparticles and multi-walled carbon nanotubes paste electrode in alkaline media for fuel cell. Int. J. Hydrogen Energy, **41**, 20085-20099 (2016)

46. S.K. Hassaninejad-Darzi, Fabrication of a non-enzymatic Ni (ii) loaded ZSM-5 nanozeolite and multi-walled carbon nanotubes paste electrode as a glucose electrochemical sensor. RSC Adv. **5**, 105707-105718 (2015)

47. K. Nagashree and M. Ahmed, Electrocatalytic oxidation of methanol on Ni modified polyaniline electrode in alkaline medium. J. Solid State Electrochem. **14**, 2307-2320 (2010)

48. A. El-Shafei, A.A. Elhafeez, and H. Mostafa, Ethanol oxidation at metal–zeolite-modified electrodes in alkaline medium. Part 2: palladium–zeolite-modified graphite electrode. J. Solid State Electrochem. **14**, 185-190 (2010)

49. M. Fleischmann, K. Korinek, and D. Pletcher, The oxidation of organic compounds at a nickel anode in alkaline solution. J. Electroanal. Chem. Inter. Electrochem. **31**, 39-49 (1971)

50. S. Hassaninejad-Darzi, M. Rahimnejad, and M. Golami-Esfidvajani, Electrocatalytic Oxidation of Formaldehyde onto Carbon Paste Electrode Modified with Nickel Decorated Nanoporous Cobalt-Nickel Phosphate Molecular Sieve for Fuel Cell. Fuel Cells, **16**, 89-99 (2016)

51. S.K. Hassaninejad-Darzi, et al., Electrocatalytic Oxidation of Formaldehyde onto Carbon Paste Electrode Modified with Hydrogen Titanate Nanotubes, Including Nickel Hydroxide. Iran. J. Sci. Technol. A, **42**, 1259-1268 (2018)

52. H. Bode, K. Dehmelt, and J. Witte, Zur kenntnis der nickelhydroxidelektrode-I. Über das nickel (II)-hydroxidhydrat. Electrochim. Acta, **11**, 1079-IN1 (1966)

53. A. Ciszewski and G. Milczarek, Kinetics of electrocatalytic oxidation of formaldehyde on a nickel porphyrin-based glassy carbon electrode. J. Electroanal. Chem. **469**, 18-26 (1999)

54. H. Yang, et al., Electrocatalytic mechanism for formaldehyde oxidation on the highly dispersed gold microparticles and the surface characteristics of the electrode. J. Mol. Catal. A: Chem. **144**, 315-321 (1999)

55. M. Koper, M. Hachkar, and B. Beden, Investigation of the oscillatory electro-oxidation of formaldehyde on Pt and Rh electrodes by cyclic voltammetry, impedance spectroscopy and the electrochemical quartz crystal microbalance. J. Chem. Soc., Faraday Trans. **92**, 3975-3982 (1996)

56. G. Barral, S. Maximovitch, and F. Njanjo-Eyoke, Study of electrochemically formed Ni(OH)2 layers by EIS. Electrochim. Acta, **41**, 1305-1311 (1996)

57. R. Ojani, J.-B. Raoof, and S. Safshekan, Electrocatalytic oxidation of formaldehyde on nickel modified ionic liquid carbon paste electrode as a simple and efficient electrode. J. Appl. Electrochem. **42**, 81-87 (2012)

58. A. Samadi-Maybodi, S. Ghasemi, and H. Ghaffari-Rad, Application of nano-sized nanoporous zinc 2-methylimidazole metal-organic framework for electrocatalytic oxidation of methanol in alkaline solution. J. Power Sources, **303**, 379-387 (2016)

59. E. Laviron, General expression of the linear potential sweep voltammogram in the case of diffusionless electrochemical systems. J. Electroanal. Chem. Inter. Electrochem. **101**, 19-28 (1979)

60. S. Hassaninejad-Darzi, Application of Synthesized NaA Nanozeolite as a Novel Supported Electrode for the Formaldehyde Electro-catalytic Oxidation. Fuel Cells, **18**, 82-95 (2018)

61. A.J. Bard and L.R. Faulkner, *Fundamentals and applications. Electrochemical Methods, 2nd ed.;* (Wiley, New York, 2001)

62. B. Habibi and N. Delnavaz, Electrocatalytic oxidation of formic acid and formaldehyde on platinum nanoparticles decorated carbon-ceramic substrate. Int. J. Hydrogen Energy, **35**, 8831-8840 (2010)

63. C. Wang, et al., Facile fabrication of ethylene glycol intercalated cobalt-nickel layered double hydroxide nanosheets supported on nickel foam as flexible binder-free electrodes for advanced electrochemical energy storage. Electrochim. Acta, **191**, 329-336 (2016)

64. Y. Shu, et al., Facile synthesis of ultrathin nickel–cobalt phosphate 2D nanosheets with enhanced electrocatalytic activity for glucose oxidation. ACS appl. Mater. Inter. **10**, 2360-2367 (2018)

65. C.O. Laoire, et al., Elucidating the mechanism of oxygen reduction for lithium-air battery applications. J. Phys. Chem. C, **113**, 20127-20134 (2009)

66. D.K. Gosser, *Cyclic voltammetry: simulation and analysis of reaction mechanisms*. (Wiley, New York, 1993)

67. S.K. Hassaninejad-Darzi, Encapsulation of a nickel Salen complex in nanozeolite LTA as a carbon paste electrode modifier for electrocatalytic oxidation of hydrazine. Chin. J. Catal. **39**, 283-296 (2018)

68. M.S. Tohidi and A. Nezamzadeh-Ejhieh, A simple, cheap and effective methanol electrocatalyst based of Mn (II)-exchanged clinoptilolite nanoparticles. Int. J. Hydrogen Energy, **41**, 8881-8892 (2016)

69. M.S. Tohidi and A. Nezamzadeh-Ejhieh, A simple, cheap and effective methanol electrocatalyst based of Mn(II)-exchanged clinoptilolite nanoparticles. Int. J. Hydrogen Energy, **41**, 8881-8892 (2016)

70. S. Azizi, S. Ghasemi, and H. Yazdani-Sheldarrei, Synthesis of mesoporous silica (SBA-16) nanoparticles using silica extracted from stem cane ash and its application in electrocatalytic oxidation of methanol. Int. J. Hydrogen Energy, **38**, 12774-12785 (2013)

71. A. El-Shafei, Electrocatalytic oxidation of methanol at a nickel hydroxide/glassy carbon modified electrode in alkaline medium. J. Electroanal. Chem. **471**, 89-95 (1999)

72. A.J. Bard and L.R. Faulkner, Fundamentals and applications. Electrochemical Methods, (Wiley, New York, 2001)

73. H. Luo, et al., Investigation of the electrochemical and electrocatalytic behavior of single-wall carbon nanotube film on a glassy carbon electrode. Anal. Chem. **73**, 915-920 (2001)

74. Y. Yu, et al., Electrocatalytic oxidation of formaldehyde on nickel ion implanted-modified indium tin oxide electrode. J. Power Sources, **286**, 130-135 (2015)

75. R. Ojani, J.B. Raoof, and S.R.H. Zavvarmahalleh, Preparation of Ni/poly (1, 5-diaminonaphthalene)-modified carbon paste electrode; application in electrocatalytic oxidation of formaldehyde for fuel cells. J. Solid State Electrochem. **13**, 1605-1611 (2009)

76. J.-B. Raoof, et al., Highly improved electrooxidation of formaldehyde on nickel/poly (o-toluidine)/Triton X-100 film modified carbon nanotube paste electrode. Int. J. Hydrogen Energy, **37**, 2137-2146 (2012)

77. J.-B. Raoof, et al., Poly (N-methylaniline)/nickel modified carbon paste electrode as an efficient and cheep electrode for electrocatalytic oxidation of formaldehyde in alkaline medium. J. Electroanal. Chem. **633**, 153-158 (2009)

78. S.R. Hosseini, et al., Synthesis of Pt–Cu/poly (o-Anisidine) nanocomposite onto carbon paste electrode and its application for methanol oxidation. Int. J. Hydrogen Energy, **40**, 292-302 (2015)

Figures

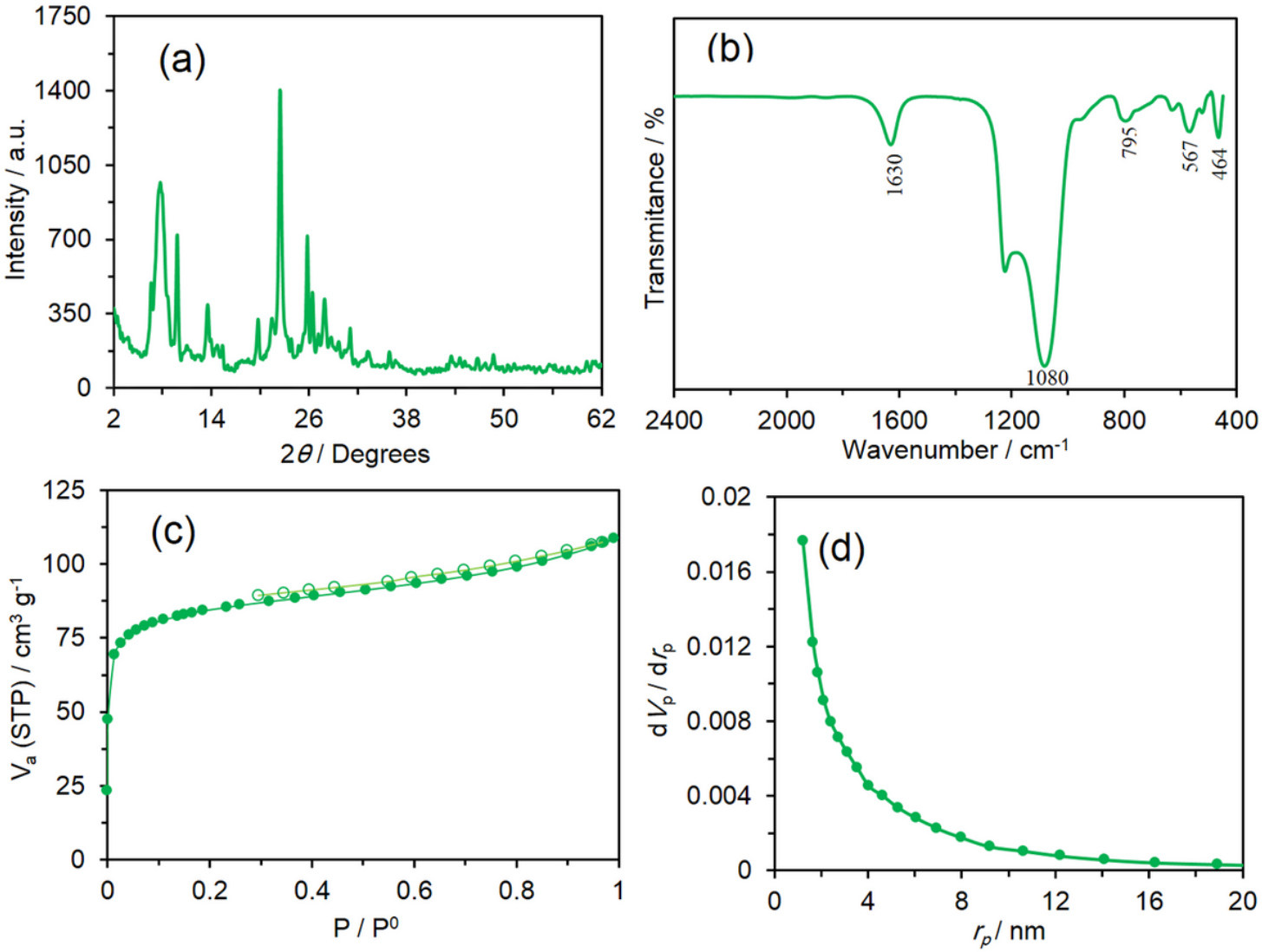

Figure 1

Representation of (a) XRD pattern, (b) FT-IR spectrum and (c) Nitrogen adsorption (close circle) and desorption (open circle) isotherms of the synthesized nanozeolite beta. (d) BJH pore size distribution from adsorption branch of isotherm

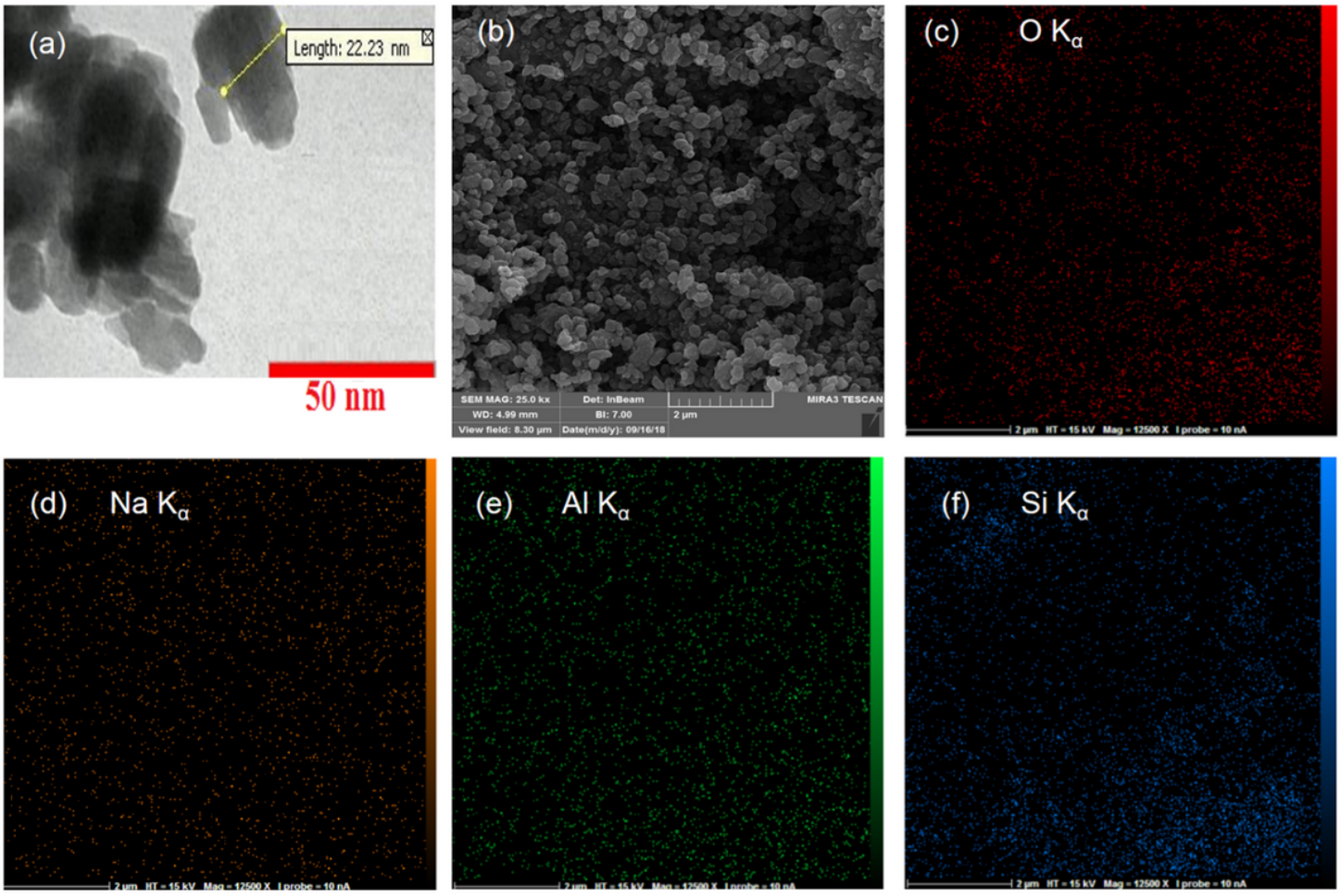

Figure 2

Representation (a) TEM image, (b) FESEM micrographs and (c-f) elemental mapping of the prepared nanozeolite beta

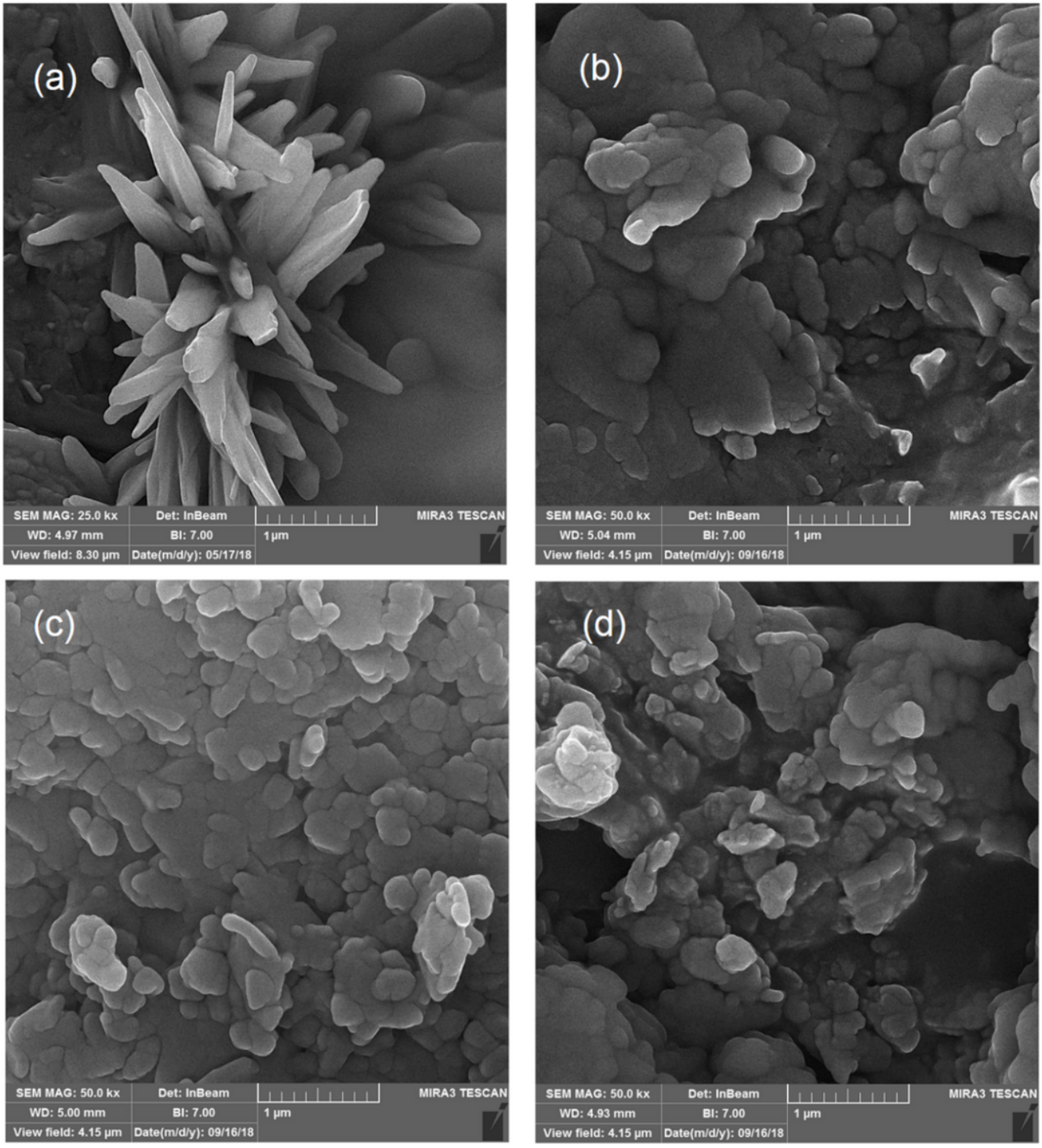

Figure 3

FESEM images of (a) CPE, (b) $Ni(OH)_2$/CPE, (c) Beta/CPE and (d) $Ni(OH)_2$-Beta/CPE

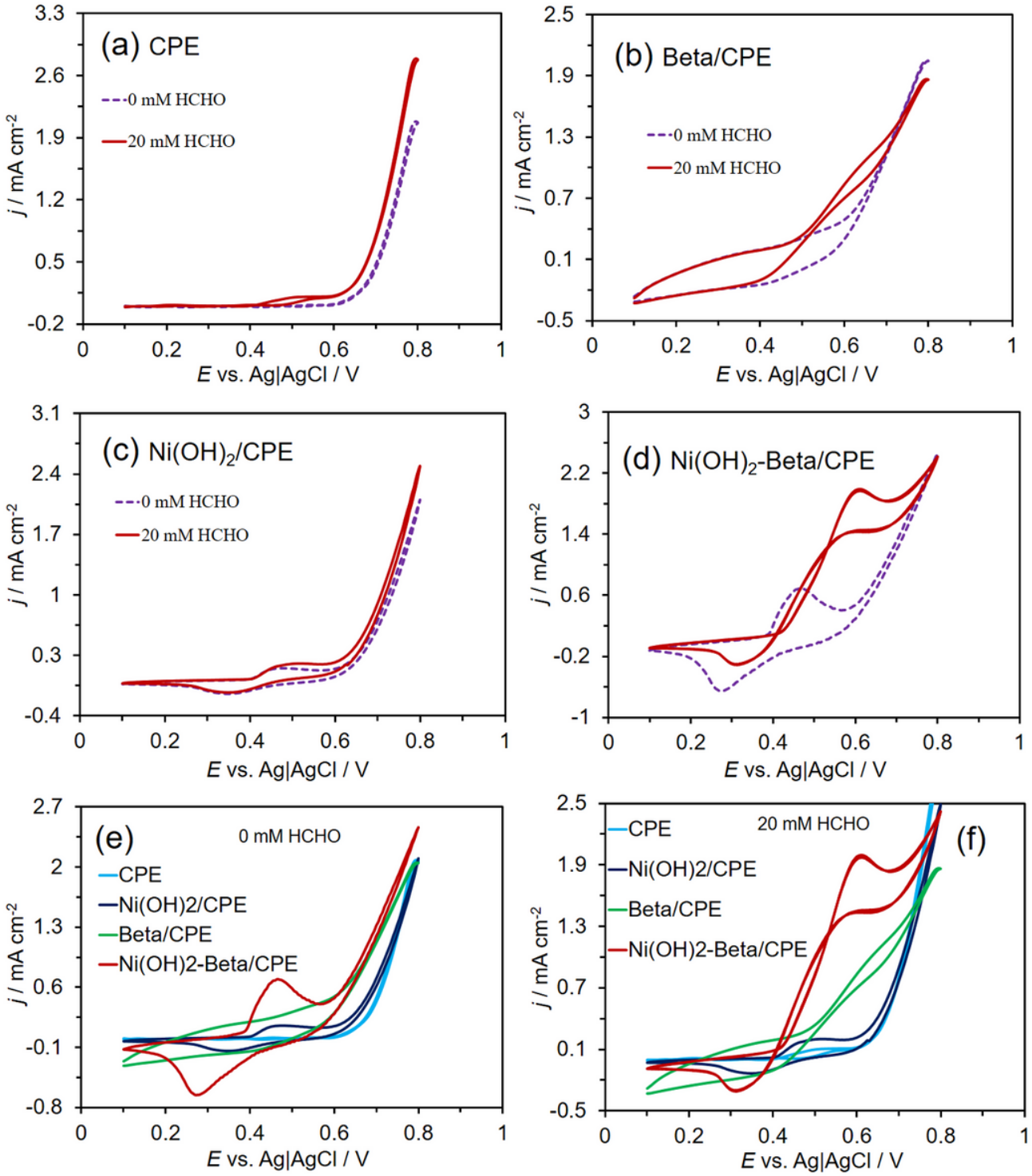

Figure 4

(a-d) Cyclic voltammograms (CVs) of all fabricated electrodes without and with 20 mM HCHO. CVs comparison of all fabricated electrodes (e) without HCHO and (f) with 20 mM HCHO. Sweep rate in all cases is 0.02 V s^{-1} and supporting electrolyte is 0.1 M NaOH

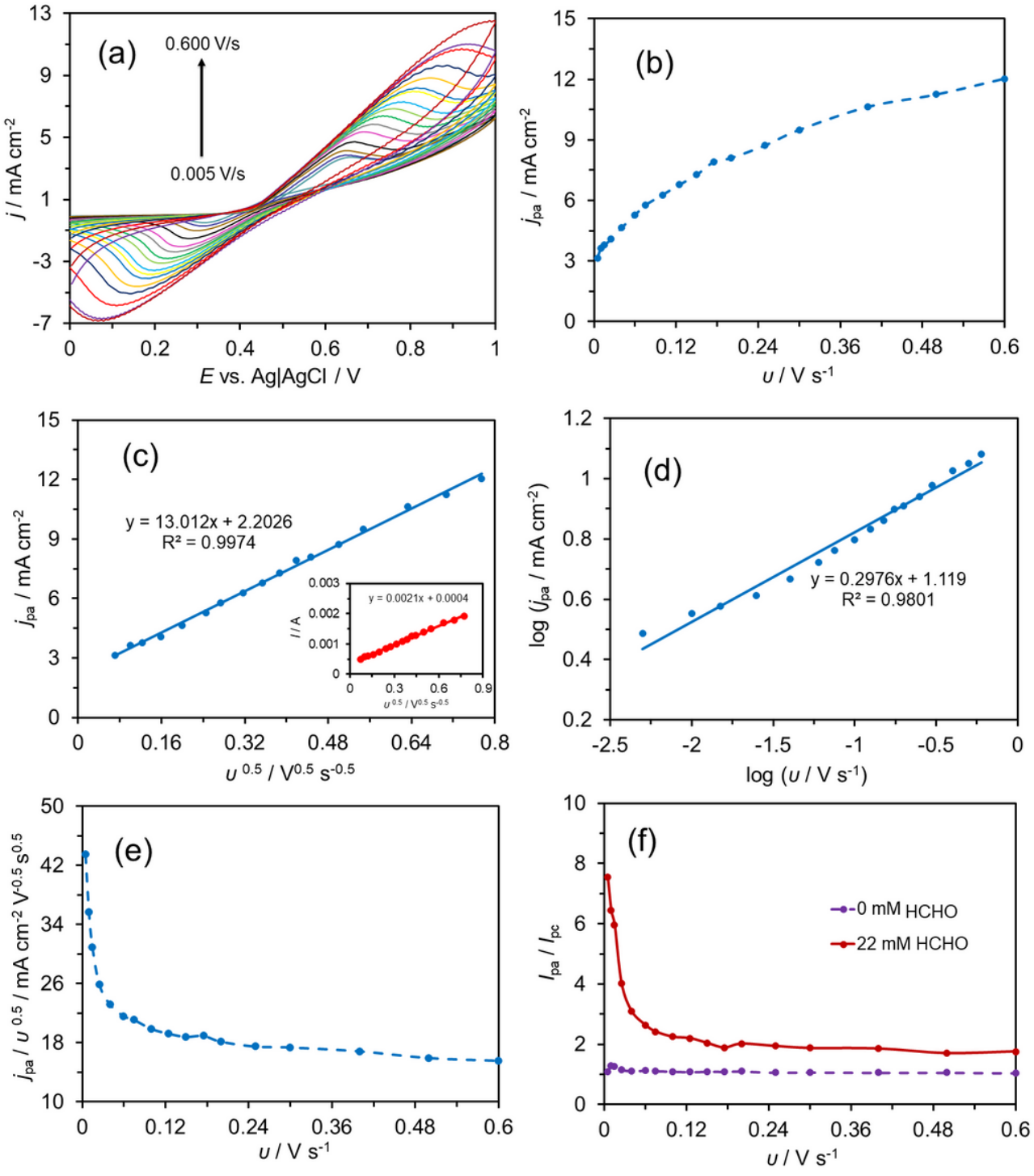

Figure 5

(a) CVs registered on $Ni(OH)_2$-Beta/CPE in 0.1 M NaOH with 22 mM HCHO at different sweep rates from inner to outer: 0.005, 0.010, 0.015, 0.025, 0.040, 0.060, 0.075, 0.100, 0.125, 0.150, 0.175, 0.200, 0.250, 0.300, 0.400, 0.500 and 0.600 V s^{-1}. Plots of (b) j_{pa} vs. υ and (c) j_{pa} vs. $\upsilon^{0.5}$, (d) log j_{pa} vs. log υ and (e) j_{pa} / $\upsilon^{0.5}$ vs. υ. Inset in (c) shows I_{pa} vs. $\upsilon^{0.5}$. (f) Variant of the I_{pa}/I_{pc} ratio with υ without and with 22 mM HCHO in 0.1 M NaOH

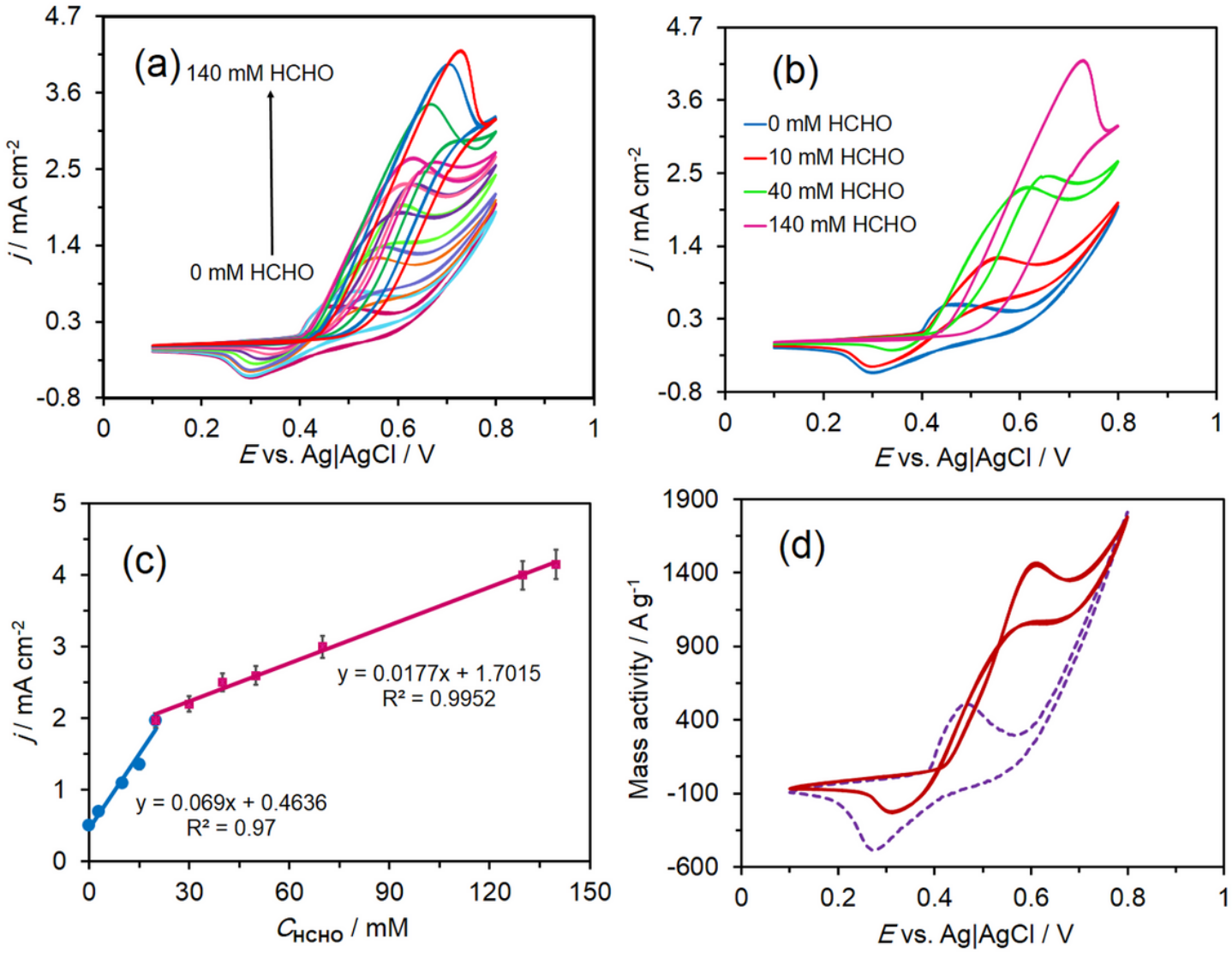

Figure 6

(a) CVs of $Ni(OH)_2$-Beta/CPE in 0.1 M NaOH at sweep rate of 0.02 V s^{-1} with various HCHO concentrations: 0, 3, 5, 10, 15, 20, 30, 40, 50, 70, 130 and 140 mM. (b) Zoomed CVs for 0, 10, 40 and 140 mM HCHO from the main panel. (c) Calibration plot for HCHO. (d) Mass activity diagram of $Ni(OH)_2$-Beta/CPE without and with 20 mM HCHO

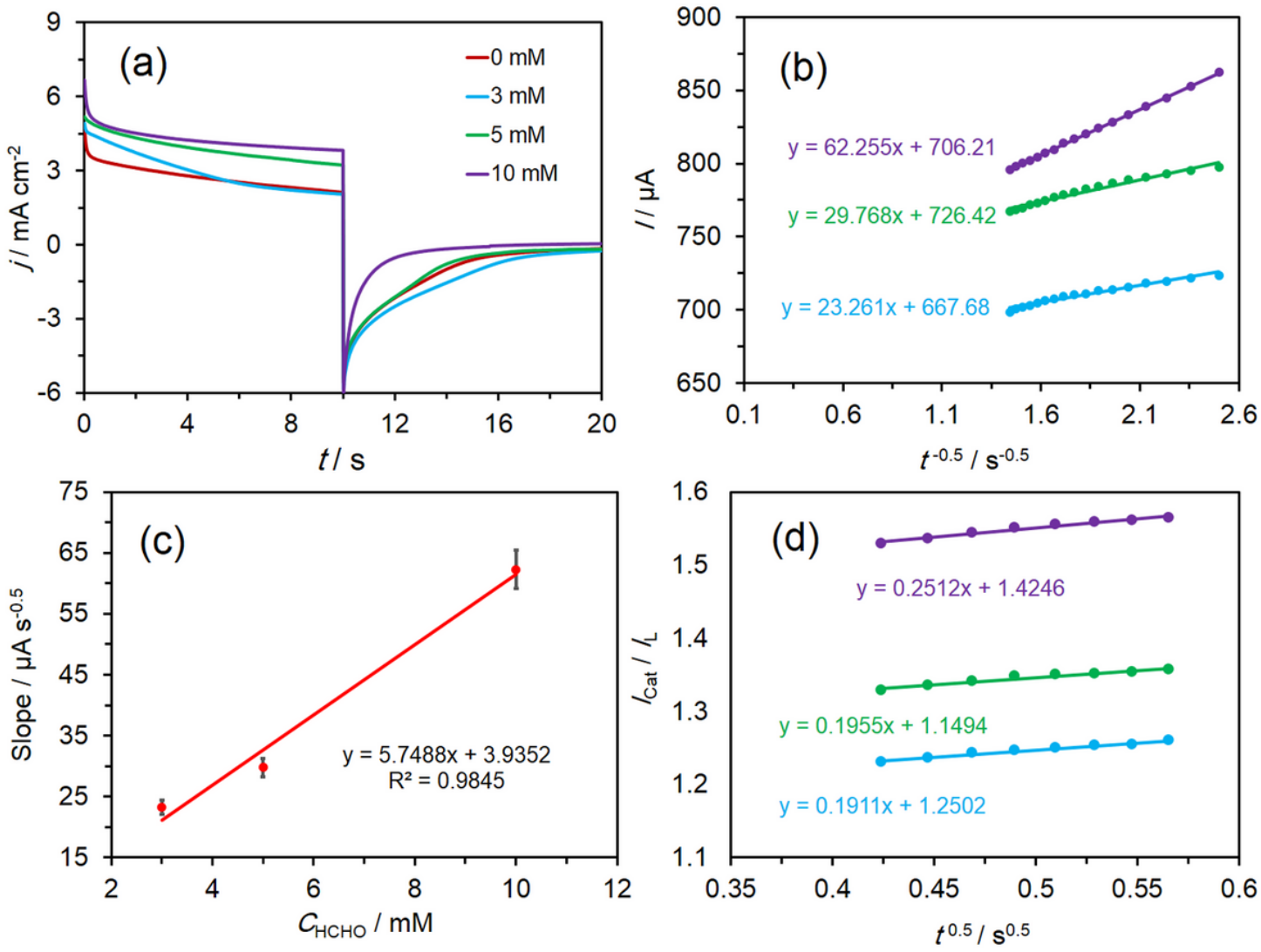

Figure 7

(a) The double step chronoamperograms of $Ni(OH)_2$-Beta/CPE in 0.1 M NaOH without and with 3, 5 and 10 mM HCHO. Curves of (b) I vs. $t^{-0.5}$, (c) slope of straight lines versus HCHO concentrations and (d) I_{cat}/I_L versus $t^{0.5}$. (The potential steps were 0.65 and 0.25 V vs. Ag|AgCl|KCl(3M))

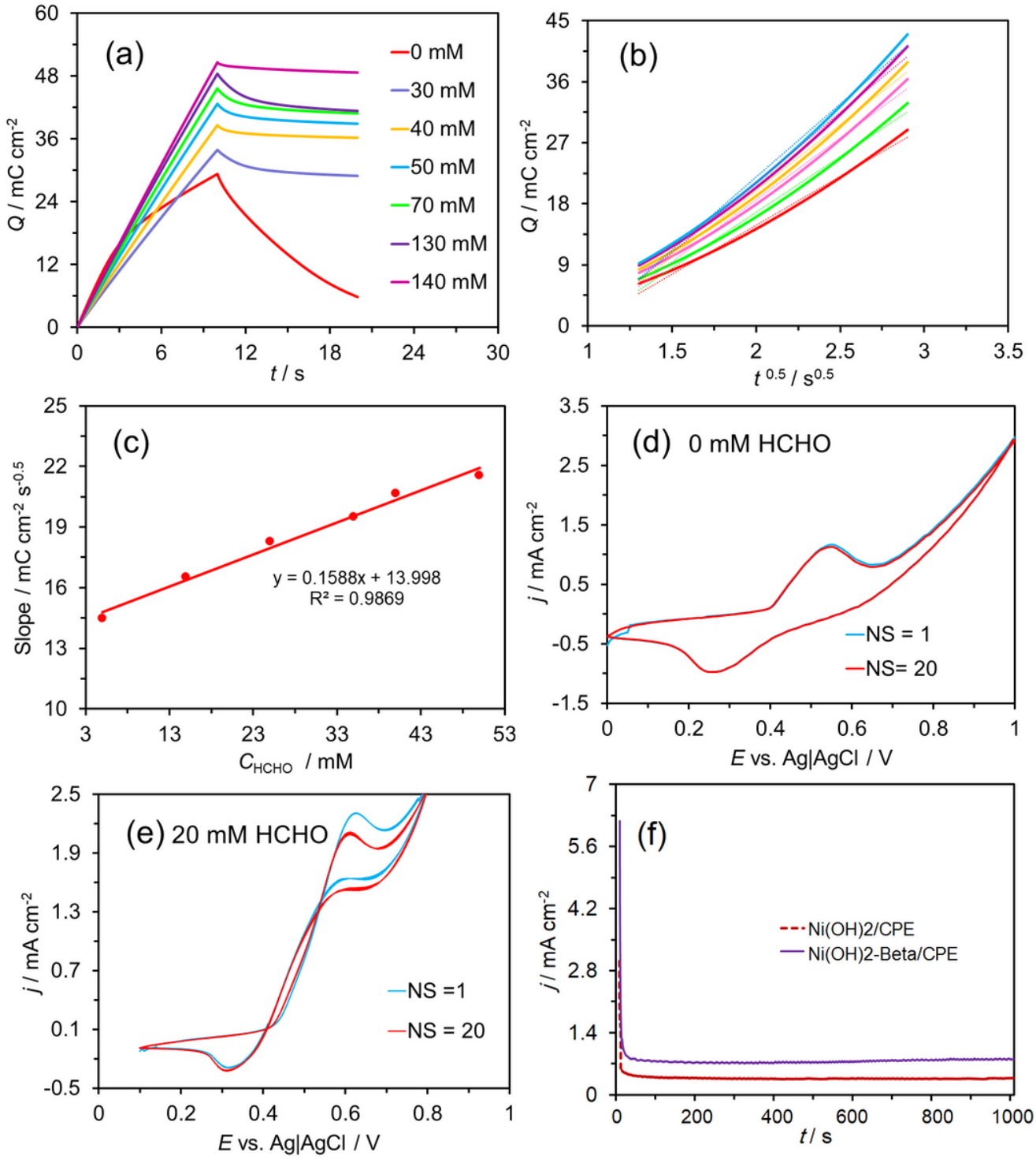

Figure 8

(a) Chronocoulomograms of the $Ni(OH)_2$-Beta/CPE in 0.1 M NaOH without and with various HCHO concentrations (The potential steps were 0.65 and 0.25 V vs. Ag|AgCl|KCl(3M)). (b) Dependency of Q on $t^{0.5}$ for all HCHO concentrations. (c) curve of the slope of straight lines versus HCHO concentration. CVs registered on $Ni(OH)_2$-Beta/CPE in 0.1 M NaOH and sweep rate of 0.05 V s^{-1} at various cycle numbers (d) without HCHO and (e) with 20 mM HCHO. (f) The current–time transient for electro-oxidation of 20 mM HCHO at the $Ni(OH)_2$/CPE and $Ni(OH)_2$-Beta/CPE surface in 0.1 M NaOH

Supplementary Files

This is a list of supplementary files associated with this preprint. Click to download.

- SupplementaryMaterial.docx